Applications in Energy and Combustion Science 17 (2024) 100254

Contents lists available at ScienceDirect

Applications in Energy and Combustion Science

journal homepage: www.elsevier.com/locate/jaecs

Ignition characteristics of hydrogen-enriched ammonia/air mixtures

Stefan Essmann [a,*], Jessica Dymke [a], Jacqueline Höltkemeier-Horstmann [a], Dieter Möckel [a], Carola Schierding [a], Michael Hilbert [a], Chunkan Yu [b], Ulrich Maas [b], Detlev Markus [a]

[a] Physikalisch-Technische Bundesanstalt (PTB), Bundesallee 100, 38116 Braunschweig, Germany
[b] Karlsruhe Institute of Technology (KIT), Institute of Technical Thermodynamics, Engelbert-Arnold-Str. 4, 76131 Karlsruhe, Germany

ARTICLE INFO

Keywords:
Ammonia
Hydrogen
Spark ignition
Explosion protection

ABSTRACT

Ammonia is an attractive hydrogen carrier and potential fuel which could play a role in decarbonizing process heat, power or transport applications. However, the combustion properties of ammonia are disadvantageous for many technical processes. Hydrogen addition has been shown to mitigate this challenge by increasing the laminar burning velocity and extending the lean blow-off limit. In this work, the ignition characteristics of hydrogen enriched ammonia/air mixtures are investigated experimentally. A capacitive discharge is used to ignite the mixture. The effects of an increasing share of hydrogen in the fuel are a drastic decrease in ignition energy as well as an increase in explosion pressure and the rate of pressure rise. Further, schlieren imaging was employed to study the structure and evolution of the flame kernel shortly after ignition. Due to the high discharge energy necessary to ignite ammonia/air, the flame kernel evolution is dominated by the discharge.

1. Introduction

The use of ammonia as a hydrogen carrier and fuel is currently discussed as one path towards the de-fossilization of the energy system [1]. Its main benefits are high energy density and lack of carbon atoms which make for an efficient, carbon-neutral energy carrier. Further, as ammonia is a widely used chemical, a worldwide infrastructure is already in place and significant experience with safe handling of ammonia exists. According to a recent study, ammonia is projected to be the most cost-effective fuel of all Power-to-X fuels currently under discussion for import to Germany [2]. The direct combustion of ammonia is an interesting application for power [3], transport [4,5] and process heat applications [1]. While ammonia combustion does not lead to emission of carbon dioxide, other emissions need to be considered. In particular, ammonia slip (NH_3) resulting from incomplete combustion, nitrous oxide (N_2O) as a very potent greenhouse gas and nitrogen oxides (NO_x) can have a large environmental and health impact [6,7]. NO_x reduction strategies have been proposed to address the latter issue [8,9]. Furthermore, the reactivity of ammonia/air mixtures is low when compared to typical hydrocarbons [10]. For instance, the laminar burning velocity is below 10 cm/s [10–13] as compared to 45 cm/s to 50 cm/s for gasoline [14]. Further, flame blow-off and frequent flame extinction may occur [15,16]. Moreover, ammonia is not easily ignited which can present a challenge in practical ignition systems [10]. This raises an issue regarding the efficiency and applicability of ammonia to existing combustion processes. A possible method to improve the burning characteristics is the addition of hydrogen [10]. Hydrogen, as a carbon free fuel, is very reactive and has a high laminar burning velocity (> 200 cm/s) [17]. This will result in better auto-ignitability [18], higher burning velocity [19] and better resistance to flame extinction [20]. Furthermore, various works have numerically investigated the spark ignition behaviour of the ammonia/hydrogen/air mixture in different geometries and under different combustion conditions based on full chemical mechanisms [20–22]. The work by Fernández-Tarrazo et al. [22] focussed on the effect of ammonia addition on the ignition energy by numerical simulations. They found an approximately exponential decrease of the ignition energy with increasing hydrogen content.

From the aspect of experimental investigation, there exist already several studies related to the ignition energy of ammonia-based combustion systems. For instance, Pfahl et al. [30] intensively measured the ignition energy of ammonia/air and ammonia/nitrous oxide/nitrogen mixtures. Lesmana et al. [29] focused on the dissociation of ammonia in air and discussed the effect of spark gap and duration on the minimum ignition energy. Oh et al. [31] studied experimentally the spark ignition behaviour of natural gas/ammonia mixtures under load conditions of spark-ignited engines. Table 1 lists previous experimental works that report on the MIE of ammonia/air mixtures and dissociated ammonia/air mixtures. The addition of hydrogen is in the scope of only two works [22,23] by means of partially dissociated ammonia. However, direct replacement of ammonia with hydrogen has not been investigated experimentally yet. Hence, there is a lack of experimental data

* Corresponding author.
E-mail address: stefan.essmann@ptb.de (S. Essmann).

https://doi.org/10.1016/j.jaecs.2024.100254
Received 15 June 2023; Received in revised form 2 December 2023; Accepted 27 January 2024
Available online 1 February 2024

Table 1
Overview of literature reporting MIE values for NH_3/air mixtures.

Mixtures	Details of experimental setup	MIE value	Reference
NH_3/air at $\phi = 0.7$ to 1.2, dissociation degree 0 % to 28 %	Cylindrical electrodes ⌀0.572 mm, high-speed steel, distance optimized for each mixture (values not given)	8 mJ at $\phi = 0.9$	Verkamp et al. [23]
NH_3/air in flammable range	3.175 mm wire electrodes	680 mJ	Buckley and Husa [24]
NH_3/air, ϕ not specified	Capacitance spark	170 mJ	Harris and MacDermott [25]
NH_3/air at $\phi = 0.7$ to 1.3	Ball electrodes ⌀5 mm, 8 mm and 15 mm, stainless steel, distance: 4 mm to 16 mm	14 mJ at $\phi = 0.9$	Krämer [26]
NH_3/air, ϕ not specified	According to ASTM E582 (2007)	15 mJ to 20 mJ	Davis et al. [27]
NH_3/air at $\phi = 0.7$ to 1.2	According to EN 1839. Cylindrical electrodes ⌀3.2 mm with 60° cone tip, tungsten, distance 5 mm	(18.0 ± 1.4) mJ at $\phi = 0.9$	Sadaghiani et al. [28]
NH_3/air at $\phi = 0.7$ to 1.2, dissociation degree 0 % to 10 %	3.0 mm wire electrodes with 28.5° cone tip, tungsten, distance 4 mm to 8 mm, spark duration 5 µs to 150 µs	18 mJ at $\phi = 0.9$	Lesmana et al. [29]

concerning the forced ignition of ammonia/hydrogen/air mixtures. Such data will be useful for designing ignition systems for practical applications, in order to validate numerical and kinetic models and finally, to assess the explosion risk connected to these mixtures.

For a detailed description of the ignition process, a distinction must be made between the early spark-dominated phase and the subsequent self-sustained flame propagation. This work focuses on the early phase of ignition. Since the energy required for ignition differs between ammonia in air and hydrogen in air by almost three orders of magnitude (Table 2), it is also important to investigate the influence of energy on this early phase. Here, it is not only the value of the energy that is important. A higher energy also results in a larger spark radius [32,33], which has a significant influence on the energy density, which is decisive for ignition. In addition, the importance of spark assisted flame propagation depends on the energy used [34]. At a higher energy, the transition to self-sustained flame propagation occurs at larger radii. In order to better understand the ignition of NH_3/H_2/air mixtures by electrical discharges and to be able to describe them numerically in the future, it is therefore important to investigate the influences described above.

Therefore, in this study the ignition characteristics of ammonia/hydrogen/air mixtures with varying hydrogen content are examined experimentally for a given electrode configuration. The most ignitable ammonia/air mixture at equivalence ratio $\phi = 0.9$ [26] is taken as the base case. This also removes the difficulties in finding out the optimal or reasonable spark gap and duration for different fuel/air equivalent ratios. Keeping the equivalence ratio constant, mixtures with a growing content of hydrogen in the fuel are ignited using a capacitive discharge. The energy required to ignite the mixtures is in the focus of the present study. Further, the pressure evolution is analysed. Finally, schlieren imaging is employed to study the ignition process and transition to self-sustained flame propagation.

The paper is structured as follows. First, the experiment is explained and justification of the choice of experimental parameters is given. Then, the experimental results are presented. The effect of hydrogen content in the fuel on the pressure evolution, the ignition energy and the development of the flame kernel are discussed. Lastly, the implications of these results for process safety and applications of ammonia/hydrogen/air mixtures are explored.

2. Materials and methods

2.1. Choice of experimental parameters

As indicated in Table 2, the minimum ignition energy (MIE) of ammonia and hydrogen differ by three orders of magnitude. It is, therefore, challenging to choose experimental conditions that allow for ignition of all possible mixtures close to the MIE. For this, several parameters such as the electrode distance, electrode geometry, and discharge characteristics would need to be optimized for each mixture composition. It is important to note that there are various definitions of the MIE in the literature. For combustion applications such as internal combustion engines, where ignition is desired, the MIE is often interpreted as the energy which leads to ignition with 50 % probability [35]. In process safety, it is defined at 1 % probability [36]. In this work, we will follow the latter definition. The goal of this work is explicitly not to determine the MIE of ammonia/hydrogen/air mixtures but to investigate the influence of hydrogen content in the fuel on the ignition characteristics in general, i.e. the explosion pressure, the ignition energy and the flame kernel development. The experimental parameters that need to be defined are the mixture composition and the electrodes (shape, material and distance).

Table 2
Safety characteristic parameters of ammonia and hydrogen. Data from *Chemsafe* database [37]. Note that the maximum explosion pressure is the absolute pressure after ignition at atmospheric conditions.

	NH_3	H_2
Max. explosion pressure	6.9 bar	8.3 bar
Most ignitable mixture	20 vol%	22 vol%
Lower explosion limit	14 vol%	4 vol%
Upper explosion limit	32.5 vol%	77 vol%
Minimum ignition energy	14 mJ	0.017 mJ

2.1.1. Mixture composition

Existing works indicate that even small hydrogen admixtures of 10 % to 20 % significantly change the burning characteristics of the gas mixture [10,15,19,38]. This could extend the application possibilities of ammonia-based fuels [1,10]. The hydrogen content of the gas mixture will be expressed in terms of its mole fraction in the fuel α_{H_2} according to the global reaction equation:

$$\alpha_{H_2}H_2 + \left(1-\alpha_{H_2}\right)NH_3 + \frac{3-\alpha_{H_2}}{4}\left(O_2 + 3.76N_2\right) \rightarrow \frac{\alpha_{H_2}+2}{3}H_2O + \left(3.32 - 1.44\alpha_{H_2}\right)N_2 \quad (1)$$

For ammonia, the most ignitable mixture is at equivalence ratio $\phi = 0.9$ while for hydrogen, it is more lean at $\phi = 0.7$ (Table 2). However, the ignition limit curve of hydrogen is very flat between $\phi = 0.7$ and $\phi = 1.0$. Hence, it is expected that the most ignitable equivalence ratio for ammonia/air mixtures with small admixtures of hydrogen is close to $\phi = 0.9$ and the mixtures investigated are chosen at this equivalence ratio. α_{H_2} is varied in the range 0 to 0.2. This range is relevant for technical applications of ammonia/hydrogen/air mixtures [39,40],

Table 3
Mole fractions of species in investigated mixtures (ϕ = 0.9).

α_{H_2}	Mole fraction	
	NH_3	H_2
0.000	0.201	0.0
0.025	0.198	0.005
0.049	0.194	0.010
0.075	0.190	0.015
0.099	0.186	0.021
0.125	0.182	0.026
0.150	0.178	0.031
0.175	0.174	0.037
0.200	0.170	0.043
1.000	0.0	0.274

even though higher concentrations of hydrogen have also been used successfully [3,41,42]. It will be seen later that this range is sensible for the selected experimental parameters. In addition, $\alpha_{H_2} = 1$ is investigated as a reference case. The mole fractions of the chosen gas mixtures are listed in Table 3.

Before digging into the influence of the hydrogen content α_{H_2} on the spark ignition process, it is worth re-visiting how some important combustion properties depends on α_{H_2}, which would help us to better understand the ignition characteristics. Fig. 1 shows the adiabatic flame temperature T_{ad} of ammonia/hydrogen/air mixtures as a function of α_{H_2} alongside several further parameters. T_{ad} was calculated using *Cantera* [43] and the thermodynamic data of Okafor et al. [44]. For the mixtures investigated here, where $\phi = 0.9$ is kept constant, T_{ad} is between 1980 K and 2300 K and increases with α_{H_2}. The flame thickness ΔF was determined from a stationary 1D flame simulation using *Cantera* by placing a tangent in the turning point of the temperature profile and finding the intersections of this tangent with the burned and unburned gas temperature. The flame thickness is the length on the abscissa between these intersection points [45]. It decreases almost linearly as α_{H_2} is increased from 0 to 0.6. For $\alpha_{H_2} > 0.8$, it is nearly constant. On the other hand, the laminar burning velocity u_L – calculated from the same stationary 1D flame simulation – increases with α_{H_2} in a seemingly exponential fashion. For instance, u_L increases by 29 % as α_{H_2} goes from 0 to 0.1 and by 69 % as α_{H_2} is further increased to 0.2. Experimental data matches this behaviour very well [10,11,15]. This suggests faster chemical reaction with increasing α_{H_2}, leading to possible lower required spark ignition energy and faster flame propagation during the ignition process. Finally, the effective Lewis number of the mixture Le_{eff} is displayed in Fig. 1. The Lewis number is an important parameter both for combustion [46] and ignition [34,47] as it influences the behaviour of flames experiencing stretch. For the mixtures investigated in this work, Le_{eff} is smaller than unity with the exception of $\alpha_{H_2} = 0$ where $Le_{eff} = 1.03$. Therefore, positive stretch as is occurs in spherically expanding flames will enhance the flame propagation. Le_{eff} was calculated using the formulation [48,49]

$$Le_{eff} = 1 + \frac{(Le_E - 1) + (Le_D - 1)\,\mathcal{A}}{1 + \mathcal{A}}, \tag{2}$$

where Le_E and Le_D are the Lewis numbers of the excess and deficient reactants and

$$\mathcal{A} = 1 + \beta\,(\Phi - 1)\,. \tag{3}$$

Here, β is the Zel'dovich number and

$$\Phi = \begin{cases} \phi & \text{if } \phi \geq 1 \\ 1/\phi & \text{if } \phi < 1 \end{cases} \tag{4}$$

is the ratio of mass of excess-to-deficient reactants in the mixture relative to their stoichiometric mixture. The effective Lewis number for the ammonia/hydrogen fuel is calculated via [50]

$$\frac{1}{Le^*} = \frac{\alpha_{NH_3}}{Le_{NH_3}} + \frac{\alpha_{H_2}}{Le_{H_2}}, \tag{5}$$

where α_{NH_3} and α_{H_2} are the volume fractions of ammonia and hydrogen in the fuel, respectively. Le^* is then used for Le_D in Eq. (2) since $\phi < 1$. The Lewis number of the excess reactant is that of oxygen. The Zel'dovich number is calculated as [51]

$$\beta = 4\frac{T_b - T_u}{T_b - T^\circ}, \tag{6}$$

where T_b and T_u are the temperature of the burned and unburned gas, respectively, and T° is the inner layer temperature. This inner layer temperature is taken from a stationary 1D flame simulation using *Cantera* as the temperature at the maximum temperature gradient [45]. Other formulations for the effective Lewis number have been used in the literature. Bouvet et al. [52] found that the volumetric average was the best approach for hydrogen/hydrocarbon fuel blends. Zitouni et al. [13] investigated NH_3/H_2 and CH_4/H_2 blends. Here, the diffusion-based formulation gave the best results for lean mixtures. Nevertheless, the diffusion-based approach (Eq. (5)) by Dinkelacker et al. [50] was used successfully by Wang et al. [53]. During forced ignition there is a large variation of kernel temperature. Because we investigate forced ignition of mixtures initially at room temperature, we used the natural choice of defining the effective Lewis number for room temperature.

2.1.2. Electrodes

The electrode shape is a key parameter that is optimized when determining the MIE of gases [54,55]. Common choices include sharpened, flanged and spherical geometries. For hydrogen, the MIE is found with ⌀2 mm spherical electrodes spaced 0.5 mm apart [56]. In case of ammonia, only few previous works report minimum ignition energies (Table 1). The value recommended by the database *Chemsafe* [37] is 14 mJ and was found by Krämer [26]. Much higher values were found by Harris and MacDermott [25] (170 mJ) and Buckley and Husa [24] (680 mJ), though these authors state the difficulty of optimizing the electrodes to achieve the minimum energy. The work by Verkamp et al. [23] states a value of 8 mJ which is the lowest value reported to date. A value of 18 mJ was found by Sadaghiani et al. [28]. The large deviations between these works can be due to different reasons, but one important difference between these studies lies in the choice of electrodes. Buckley and Husa [24] used ⌀0.125 in (3.175 mm) wire electrodes while Verkamp et al. [23] used ⌀0.572 mm drills and Krämer [26] used different spherical electrodes (⌀5 mm, 8 mm and 15 mm). Nevertheless, the work by Krämer [26] is well-documented and the effects of electrode diameter and electrode distance were analysed. Here, the lowest energy was found with ⌀5 mm spherical electrodes spaced 15 mm apart. Based on the information available for hydrogen/air and ammonia/air mixtures, spherical electrodes with ⌀5 mm were selected. Tungsten was chosen as the electrode material owing to its higher lifetime compared with the common stainless steel electrodes. The electrode distance dictates the breakdown voltage which in turn is the main factor influencing the ignition energy. It was chosen at 4 mm to allow for the ignition energy (cf. Section 2.4) to be adjusted in the range $W = 1$ mJ to 240 mJ. A larger electrode distance would increase the lower limit of W and result in a too high value. This would prevent investigation of mixtures with large α_{H_2}. A too small electrode distance would likely increase the ignition energy for the ammonia/air mixture due to loss processes [26]. In effect, the chosen value of 4 mm is a compromise which allowed to cover ignition energies adequate for the selected gas mixtures.

2.2. Explosion vessel

The ignition experiments were carried out in a constant volume vessel which had spherical inner geometry (⌀ 100 mm, volume ≈ 0.5 L). It is temperature stabilized via integrated cooling ducts and a thermostat at (20 ± 4) °C. The electrodes (⌀ 5 mm, tungsten) were fed into the vessel from the top and bottom; the top electrode was adjustable using a micrometer screw to set the electrode gap. The positional

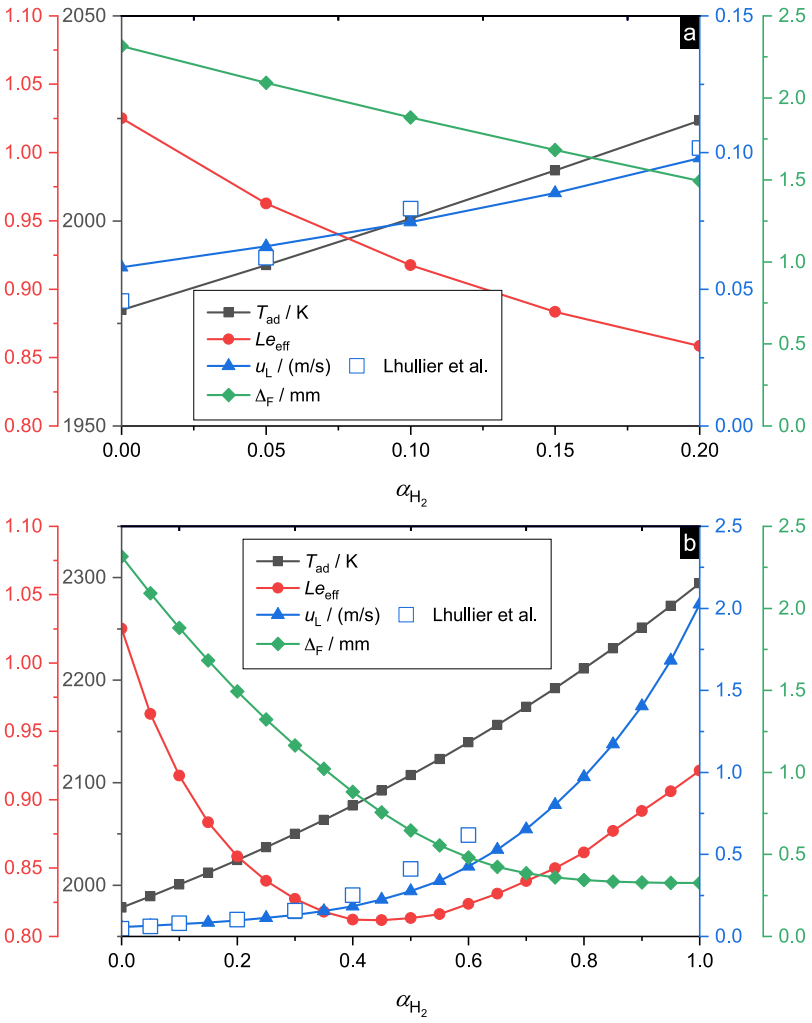

Fig. 1. Adiabatic flame temperature T_{ad}, effective Lewis number Le_{eff}, laminar burning velocity u_L and flame thickness ΔF of ammonia/hydrogen/air mixtures at $\phi = 0.9$ as a function of α_{H_2}. The experimental values for u_L are from Lhuillier et al. [11]. (a) $\alpha_{H_2} = 0 \ldots 0.2$. (b) $\alpha_{H_2} = 0 \ldots 1$.

tolerance of the electrodes (including contributions from concentricity and parallelism) was smaller than 0.1 mm. The vessel was optically accessible through eight windows with ⌀15 mm. The gas mixture in the vessel was renewed after every ignition or at most five non-ignition events during one experiment.

2.3. Mixture preparation and uncertainty

The method of partial pressures was used to prepare the mixtures (cf. Table 3) in a dedicated mixing vessel (volume 3.8 L). Prior to preparing a mixture, the whole gas-handling system was flushed with dry air (pressurized air dried in a silica gel cartridge), evacuated to below the vapour pressure of water and flushed with dry air a second time. Next, the mixing vessel was evacuated and the remaining pressure was assumed to be residual dry air. Dry air was then let into the mixing vessel until the desired partial pressure was reached. The pressure was measured with a piezoresistive pressure sensor (Kistler 4043A2) and amplifier (Kistler 4603) with a combined standard measurement uncertainty of 1 mbar. Before adding hydrogen, the gas-handling system was evacuated and flushed with hydrogen, ensuring a positive pressure gradient from the gas-handling system to the mixing vessel to avoid backflow from the mixing vessel. Then, hydrogen was let into the mixing vessel. Lastly, ammonia was added in the same fashion. The volume of the prepared mixture was sufficient to perform five experiments without the need to prepare another batch. Hence, the uncertainty of the mixture preparation does not include the repeatability of the process.

To avoid real gas effects from significantly influencing the molar composition of the mixture, the maximum pressure in the mixing vessel was kept below 2 bar. It was determined using *Refprop* [57] that for mixtures of air, hydrogen and ammonia, the compressibility factor as a measure of non-ideal behaviour does not deviate from unity by more than 0.1 % at room temperature and maximum pressures of the prepared mixtures below 3.4 bar. Further, care was taken to minimize effects by different temperatures of the gases. To this end, all gases were led through 6 m long spiral pipes and their temperature was controlled via a type K thermocouple. The gas qualities were 5.0 for ammonia and 3.0 for hydrogen. The air was taken from the pressurized air outlet and dried in a desiccant cartridge. Overall, the uncertainty in α_{H_2} was at most 0.5 vol% (absolute) or, expressed in terms of the equivalence ratio, $\phi = 0.900 \pm 0.002$.

2.4. Ignition system

The gas mixtures were ignited by a capacitive discharge. Its energy can be estimated by the energy stored in the capacitor and stray capacitances,

$$W = \frac{1}{2} C V^2, \tag{7}$$

where C is the capacitance and V is the breakdown voltage. The energy determined according to Eq. (7) is an upper bound for the actual energy

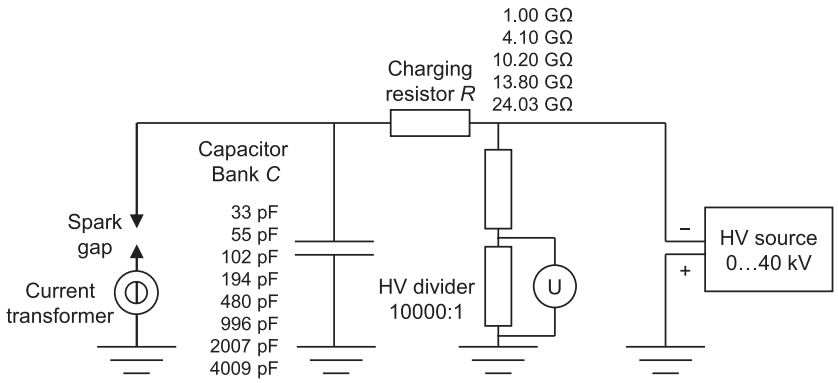

Fig. 2. Electrical setup.

of the discharge as there is always a fraction of remaining charge on the capacitor. For small values of W the energy transfer is close to 100 %. However, substantial external ohmic losses are to be expected when $W > 10$ mJ [58].

The electrical setup used to generate the discharges is shown in Fig. 2. It consisted of a high voltage source (FuG HCN40M-40000), a charging resistor R (variable) and an induction-free capacitor bank C. The charging time constant of the capacitor is

$$\tau = RC, \tag{8}$$

where R is the resistance. The charging time of the capacitor to 99.3 % is 5τ. The breakdown voltage was slightly different for each mixture (change of α_{H_2}) due to the different dielectric strengths of the gases. When the mixture was kept constant (α_{H_2} constant) the breakdown voltage was also constant since the electrode distance was fixed at 4 mm in this work. Hence, the capacity C was adjusted to vary the energy of the discharge W according to Eq. (7). C was measured with a handheld LCR meter (Agilent U1733C), R was then selected to keep τ between 2 s and 5 s. This was a compromise between charging times that were manageable (small τ desired) and sufficient time between discharges, ensuring that no compound effect from multiple discharges in a short time frame could occur (large τ desired). A high voltage divider (Spellman HVD-100, 10000:1) and a digital multimeter (Agilent 34410 A) were used to measure the voltage. The voltage divider was placed before the charging resistor on purpose. If it had been placed after the resistor, the small current draw from the voltage divider would have resulted in a significant voltage drop across the charging resistor. It would have been impossible to achieve the breakdown voltage at the spark gap. However, this placement of the voltage divider required that the voltage was increased very slowly to ensure that the capacitor was fully charged (cf. Eq. (8)) so there was virtually no current across the charging resistor. Then, it can be assumed that the voltage across the electrodes is the same as that measured by the voltage divider and measurement with a high voltage probe were done to confirm this. Further, a UV LED (Thorlabs LED250J) was positioned close to one of the windows of the vessel pointed at the electrodes and electrode gap. This was done to ensure that there was always a sufficient number of start electrons for the discharge. Indeed, preliminary tests showed that the breakdown voltage was fluctuating by more than 1 kV when the LED was off. With the LED turned on, the variance in the breakdown voltage was less than 100 V. Lastly, a current transformer (Magnelab CT-C1.0-B) was used to detect the discharge current.

2.5. Pressure measurement

The explosion pressure was measured with a piezoresistive pressure transducer (Kistler 4011 A, maximum pressure 10 bar) and amplifier (Kistler 4624 A) and recorded on an oscilloscope (Yokogawa DLM2054). While piezoelectric pressure sensors are usually preferable when measuring explosion pressure [59], in this specific case a piezoresistive pressure sensor can be used. The reason is that the geometry of the vessel is a simple sphere and no complicated flow patterns are to be expected in the relevant time frame. Hence, the frequency response of the chosen pressure transducer is sufficient to measure the explosion pressure. The added benefit is that a single pressure transducer could be used for measuring the initial pressure (static) and the explosion pressure (dynamic). A 5 kHz low-pass filter was configured on the amplifier to avoid aliasing effects [60]. The combined measurement uncertainty of the pressure measurement chain was < 5.4 % or < 0.23 bar across all experiments.

2.6. Schlieren imaging and analysis

A schlieren imaging setup was employed to visualize the ignition phase and the early flame propagation at 30 000 fps. It consisted of a red LED (MTPS8065PT) with a central wavelength of 650 nm, two field lenses ($f = 162$ mm and $f = 500$ mm), a knife edge as the schlieren stop and a high-speed camera (Photron SA5 colour) equipped with a zoom lens (Sigma AF DL, 75–300 mm). The LED was chosen to match the maximum quantum efficiency of the camera. Due to its small emitting diameter (80 µm) and emitting angle (±5° half intensity) it can be treated as a point source and no aperture is required. The resolution of the system was determined to be 28 px/mm based on the diameter of the electrodes. In order to relate the discharge to the schlieren images, the exposure signal of the camera was recorded on the same oscilloscope as the discharge current. The images were analysed as follows:

1. Background correction: Take the mean of the frames preceding the spark and divide all following frames by this mean image. A correction factor was applied to scale the mean intensity of each image equal to 1.
2. Masking: The mean image from step 1 is used to generate a mask which is applied to the dataset.
3. Find the kernel radius:
   (a) For each row smooth the intensity profile, take its derivative, smooth it and find the first extreme from either edge, corresponding to the inflection points of the intensity profile (Fig. 3), following the approach in [61].
   (b) To eliminate rows that do not contain the kernel, take only rows with an intensity maximum $I/I_0 > 1.05$ and a minimum $I/I_0 < 0.85$ as well as maximum in the first derivative of intensity four times higher than the noise.
   (c) Find the row with the maximal distance between the two maxima.
   (d) Divide the distance found this way by 2 to find the kernel radius. The uncertainty of the kernel radius is typically < 0.1 mm.

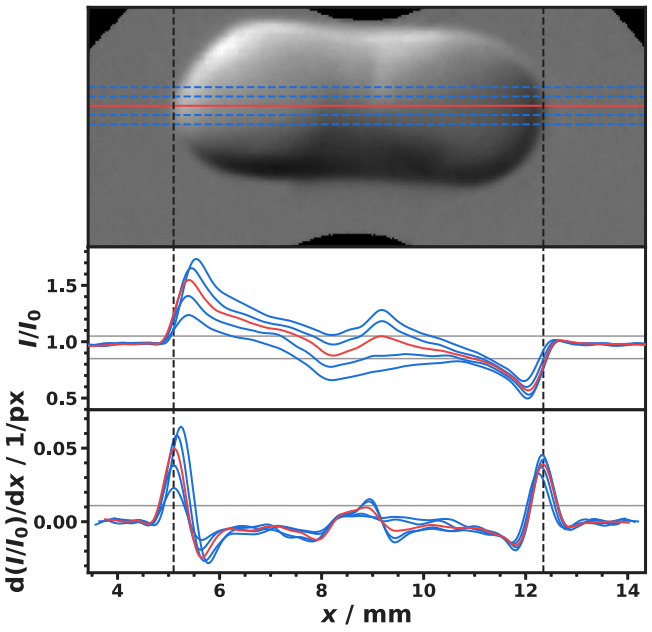

Fig. 3. Analysis of the schlieren images. Top: Schlieren image after background correction and masking. Middle: Intensity profiles after Gaussian smoothing and Savitzky–Golay filtering. Bottom: First derivative of the intensity profiles taking the smoothed and filtered data from the image above and again filtered. Red line: Row with maximum kernel radius. Blue lines: Exemplary rows close to the row with maximum kernel radius. Black dashed lines: Kernel diameter. (For interpretation of the references to color in this figure legend, the reader is referred to the web version of this article.)

4. Plot the kernel radius over time and fit it using the function $r(t) = a_1 + (a_2 t + a_3) \cdot (1 - \exp(-a_4 t))$, where r is the radius, t is time and $a_1 \dots a_4$ are fit parameters. For the $\alpha_{H_2} = 1$ mixture use a linear fit.
5. Calculate the first derivative to find $\mathrm{d}r/\mathrm{d}t$.

3. Results and discussion

3.1. Explosion pressure and rate of pressure rise

Fig. 4 shows the explosion pressure traces for the different amounts of hydrogen addition. Small hydrogen contents already significantly increase the maximum pressure as well as the rate of pressure rise. These parameters are plotted in Fig. 5. The rate of pressure rise $\mathrm{d}p/\mathrm{d}t$ was determined from the gradient of pressure from 10 % to 90 % of its maximum value. Both show a nearly linear dependency on α_{H_2} for the range $\alpha_{H_2} = 0 \dots 0.2$. For $\alpha_{H_2} = 0.2$, the maximum pressure is about twice that of the ammonia/air mixture at (6.1 ± 0.2) bar and (3.5 ± 0.2) bar, respectively. It then further increases to (7.4 ± 0.2) bar at $\alpha_{H_2} = 1$ (no ammonia in the mixture). The rate of pressure rise increases from 22 bar/s for the ammonia/air mixture to more than 100 bar/s for $\alpha_{H_2} = 0.2$. At $\alpha_{H_2} = 1$, the rate of pressure rise is dramatically higher at nearly 3500 bar/s. Overall, the maximum explosion pressure is lower than the literature values (Table 2). This is likely due to the fact that the vessel used in this work has a rather small volume (0.5 L) and the maximum explosion pressure is usually determined in a much larger vessel of at least 5 L volume [62]. For smaller volumes, the effect of the walls on the flame propagation and on the explosion pressure may be more significant [58]. As an example, the explosion pressure for $\alpha_{H_2} = 0$ is 3.5 bar in this experiment ($\phi = 0.9$). The maximum explosion pressures found by other authors are 4.9 bar in a 5 L cylindrical vessel by Di Sarli et al. [63] and 5.0 bar in a 14 L spherical chamber by Li et al. [64], both at $\phi = 1$, as well as 4.4 bar in a 20 L semi-spherical vessel by Davis et al. [27] (ϕ not reported). Another interesting aspect

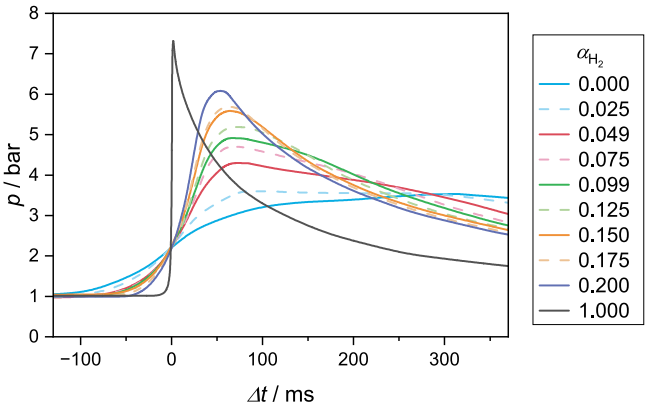

Fig. 4. Explosion pressure for varying α_{H_2}. The pressure trace for the experiment with lowest ignition energy for each fuel composition is shown. The time 0 ms corresponds to the trigger of the oscilloscope which was set at 2.2 bar (much larger than the noise level but smaller than the expected maximum pressure).

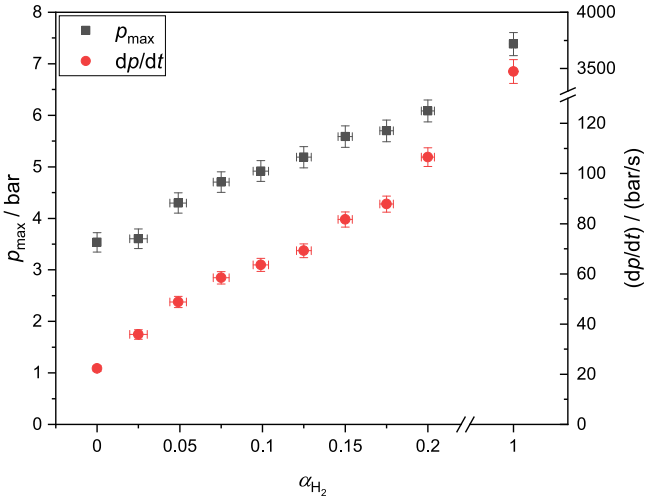

Fig. 5. Maximum pressure and rate of pressure rise for varying α_{H_2}. The experiment with lowest ignition energy for each fuel composition is shown. The error bars indicate the measurement uncertainty.

is the shape of the pressure traces for small α_{H_2}. For $\alpha_{H_2} = 0$ a two-step pressure rise is evident. A possible reason is the impact of buoyancy which makes the flame kernel rise to the top of the vessel. Once the flame reaches the top, the further combustion is limited by the walls, resulting in a decrease of the rate of pressure rise.

3.2. Ignition energy

The influence of hydrogen mole fraction in the fuel on the ignition energy is shown in Fig. 6. Here, the smallest value leading to ignition and the highest energy value which did not lead to ignition in five sparks are indicated. It is evident that even a small proportion of hydrogen in the mixture with ammonia in air leads to a significant decrease in the energy required for ignition. For example, at $\alpha_{H_2} = 0.099$ the ignition energy is reduced by a factor of 10. This result is expected and in the same order of magnitude as the results by Verkamp et al. [23]. The ammonia/air mixture ($\alpha_{H_2} = 0$) was ignited at $W = 114.5$ mJ. This value is close to the value given by Krämer [26] under the same conditions.

The energy plateaus that are visible in Fig. 6, for instance at $\alpha_{H_2} = 0.05$ and 0.075, are due to the discrete capacitance values that can be chosen from the capacitor bank. These were interchangeable with a

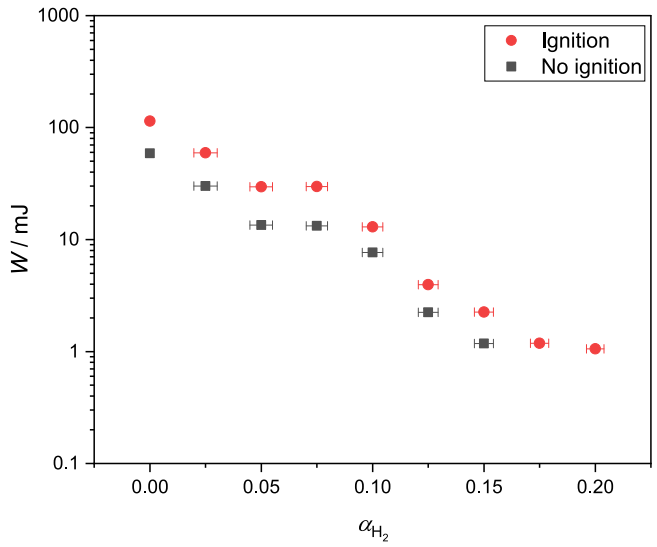

Fig. 6. Ignition and non-ignition for varying α_{H_2}. The uncertainty in W is smaller than the symbol size.

factor of 2 (Fig. 2). It is important to note that the ignition energies shown in Fig. 6 are not minimum ignition energies (MIE). To determine the MIE, an optimization of the electrode geometry and distance is required for every α_{H_2} and a large number of experiments according to the standard ASTM E582 [36] would be needed which is beyond the scope of this work. Rather, the general trend can be obtained from this data and the values are specific to the chosen setup. Energies below 1 mJ were not achievable with the chosen setup for the reasons given in Section 2.1. The ignitions for $\alpha_{H_2} = 0.175$ and 0.200 occurred with no additional capacitance and represent the minimum discharge energy which can be achieved for the chosen electrode configuration. Hence, no effect of α_{H_2} on the ignition energy was observed for $\alpha_{H_2} > 0.175$, which is clearly a limitation of the experiment. It is expected that the ignition energy will further reduce with increasing α_{H_2} (the MIE of hydrogen is 17 µJ). The electrode distance would need to be reduced to arrive at such low energy values.

The measurement uncertainty of W based on Eq. (7) is too small to be conceivable in this plot. However, the fraction of remaining charge on the capacitor bank is not known and could be significant, especially at high values of W. Hence, the data points in Fig. 6 represent an upper bound of the energy transferred to the gas mixture in the discharge.

3.3. Flame kernel development

Schlieren images of the ignition and flame kernel development are shown in Fig. 7. Due to the strongly deviating kernel growth rates, the time interval between the frames shown is different for each configuration. Also, note that the schlieren images represent the experiment with the lowest achieved ignition energy for the specific mixture composition. Hence, W is largest for $\alpha_{H_2} = 0$ and smallest for $\alpha_{H_2} = 0.2$. This effect of ignition energy is well observable in the first frame shown. For $\alpha_{H_2} = 0.15$ and 0.20 the initial kernel is cylindrical. As α_{H_2} is reduced (and W is increased), the discharge channel becomes visible as a bright line. Both the discharge radius and the heated channel radius increase. For the highest ignition energies, the heated channel grows so rapidly that already in the first frame a non-cylindrical shape is observed. The transformation from a cylindrical to a more compact (approximately spherical) shape occurs on different time scales, depending on the ignition energy and mixture composition. Due to the arrangement of the electrodes (vertical rather than horizontal), the top electrode may interfere with the flame propagation for buoyant flames. On the other hand, the arrangement ensures minimal interference of the electrodes with the kernel radii determined according to Section 2.6.

For the cases $\alpha_{H_2} = 0.049$, 0.099 and 0.150 a toroidal flame shape is observed as the kernel radius increases. Yet it becomes less clear as α_{H_2} increases. At $\alpha_{H_2} = 0.2$, this effect is not visible. Generally speaking, the flame shape is governed by the relative contributions from burning velocity and flow velocity as well as its interaction with stretch. For the mixtures considered here, $Le_{\text{eff}} < 1$. Thus, the flame propagation is enhanced by positive stretch rates. In the case of spark ignition, the flow is induced by the discharge and the flow velocity scales with the discharge energy [65]. Its properties are further influenced by the electrode shape and configuration [66,67]. As α_{H_2} is increased, the burning velocity increases significantly (Fig. 1). At the same time W is decreased, leading to a weaker flow field induced by the discharge. Both effects combined change the ratio of burning velocity and flow velocity substantially, resulting in the observed change of flame structure from toroidal to spherical as α_{H_2} is increased. However, as W is decreased by a factor of 100 (114.5 mJ to 1.1 mJ) and u_L increases by only a factor of < 2 (0.058 m/s to 0.098 m/s), the change in W must be seen as the dominating factor here. For $\alpha_{H_2} = 0$ the toroidal flame shape is also present. Here, the transition occurs very fast due to the high ignition energy $W = 114.5$ mJ and low burning velocity. It can be seen already in the third and fourth frame (113 µs and 213 µs). Due to the strong flow, the flame is perturbed more than in the other cases and appears less symmetric. Nevertheless, it is known that the vorticity induced by the discharge and hence the outward jet velocity are dependent on the electrode distance [68]. As the electrode distance was kept constant in this work, it is not possible to isolate the effects of W and α_{H_2} on the kernel shape.

The kernel radii extracted from the schlieren images and their derivatives are displayed in Fig. 8. Note that both α_{H_2} and W are varied at the same time. The main differences between the datasets stem from the vastly different discharge energies. For small α_{H_2}, a large energy is necessary to ignite the mixture. One effect of large W is that the initial radius detected in the schlieren images is much larger, e.g., 3 mm at $W = 114.5$ mJ as compared to 1 mm at $W = 13.0$ mJ. This has been observed before, albeit at much lower energy levels, for capacitive discharges in air [33]. Further, the kernel evolution is dominated by the discharge for most datasets shown. This regime is known as *spark assisted flame propagation* [69]. For the mixtures with relatively high $\alpha_{H_2} > 0.1$, the transition to a self-sustained flame propagation is captured. This is indicated by the approximately linear gradient and a nearly constant propagation speed. The mixtures with $\alpha_{H_2} < 0.1$ also exhibit this behaviour, but it was not observed in this experiment due to the limited field of view of the schlieren setup. A special case is the $\alpha_{H_2} = 1$ mixture. Here, W is much greater than the MIE and the mixture instantly ignites. Nevertheless, the laminar burning velocity of hydrogen is so large that the spark assisted flame propagation is barely noticeable. The comparison with $\alpha_{H_2} = 0$ again emphasizes how disparate the ignition and burning characteristics of hydrogen and ammonia are. Overall, it is not possible to separate the effects of hydrogen addition and discharge energy on the kernel evolution from the data in Fig. 8.

Hence, Fig. 9 shows the same quantities for a constant mixture composition ($\alpha_{H_2} = 0.099$) and two discharge energies. The same effects as described above are clearly visible, i.e., the initial radius is larger and the initial speed $\mathrm{d}r/\mathrm{d}t$ also increases with W. As the radius increases, the kernel growth rates for both cases approach each other. After around 1 ms or at a radius of 4 mm, the effect of spark ignition is not noticeable any more in $\mathrm{d}r/\mathrm{d}t$.

Comparing the plateau values of the radial expansion speed found in Fig. 8 (> 1 m/s) with literature values and numerical simulations (< 0.2 m/s, cf. Fig. 1), the speeds obtained here are much higher. This is mainly due to the curvature of the flame at this early stage which needs to be accounted for. Further, the evaluated radius range is too small and researchers aiming to investigate the laminar flame speed would usually omit this data from their evaluation [70,71].

α_{H_2}	W/mJ						
0.000	114.5	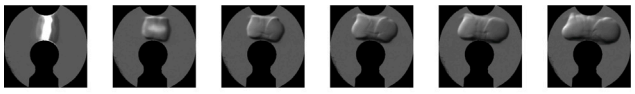	12.9 µs	46.3 µs	113 µs	213 µs	313 µs	513 µs
0.049	29.6		13.8 µs	47.1 µs	114 µs	514 µs	1014 µs	2014 µs
0.099	13.0	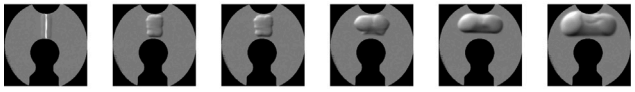	−14.5 µs	52.1 µs	85.5 µs	486 µs	986 µs	1986 µs
0.150	2.2		−0.2 µs	66.5 µs	500 µs	1000 µs	2000 µs	4000 µs
0.200	1.1	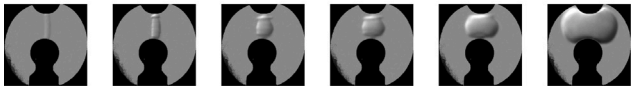	−2.0 µs	64.4 µs	498 µs	998 µs	1998 µs	3998 µs

Fig. 7. Schlieren images of the ignition and development of the flame kernel. Note the time interval between frames is different for each configuration. The time below each image is the mid-time of the frame. The exposure time for each frame was 33.3 µs so that the uncertainty for the time is ±16.7 µs. For reference, the electrode diameter is 5 mm.

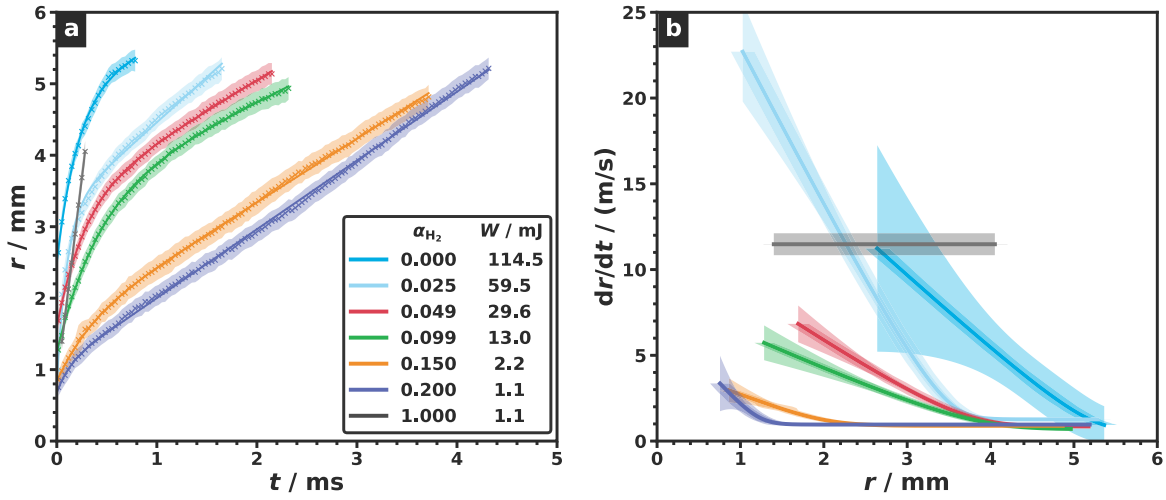

Fig. 8. Temporal evolution of the hot gas kernel for varying α_{H_2} and W. (a) Evolution of the kernel radius. (b) Change in radius plotted against the radius. The shaded areas indicate the standard measurement uncertainty.

4. Conclusions

In this work, the effect of hydrogen content in ammonia/hydrogen/air mixtures on its ignition characteristics was examined experimentally. Previous research mainly dealt with pure ammonia/air mixtures and found significantly varying minimum ignition energies. As for ammonia/hydrogen/air mixtures, only partially dissociated ammonia/air mixtures have been investigated experimentally so far. Hence, this study contributes to a better understanding of the ignition properties of ammonia/hydrogen/air mixtures under atmospheric conditions. The experimental setup was chosen to match the MIE conditions of pure ammonia as closely as possible while also allowing for the investigation of mixtures with a mole fraction of hydrogen in the fuel α_{H_2} between 0 and 0.2. The key findings were as follows:

- The maximum pressure p_{max} increases strongly with α_{H_2}.
- The rate of pressure rise dp/dt also increases with α_{H_2}.
- The ignition energy W decreases very quickly as α_{H_2} is increased (by a factor of 10 as α_{H_2} goes from 0 to 0.1).

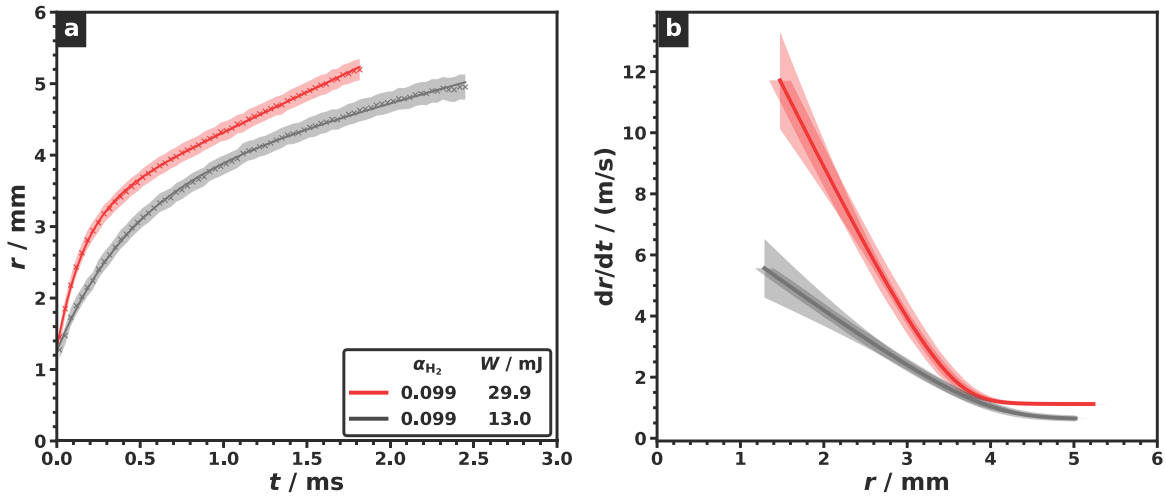

Fig. 9. Influence of discharge energy on the hot kernel. The mixture composition was kept constant at $\alpha_{H_2} = 0.099$ and the energy was varied at $W = 13.0$ mJ and 29.9 mJ. (a) Evolution of the kernel radius. (b) Change in radius plotted against the radius. The shaded areas indicate the standard measurement uncertainty.

- The early flame kernel development is dominated by the electric discharge for small α_{H_2} due to the large required ignition energy. A toroidal flame is observed for small α_{H_2}.

The results confirm the enhancement of burning characteristics which was previously reported by other authors. Hence, hydrogen blending of ammonia is a feasible way to improve its applicability to technical combustion processes. Also, the ignitability is improved already with small α_{H_2}. For desired ignition processes, this property can be used to enhance the efficiency. On the other hand, the findings should be considered for handling and utilization of ammonia/hydrogen mixtures to avoid accidents. Further research could investigate the effect of electrode shape and geometry and possibly a wider range of α_{H_2} than was possible here. Also, the results could be compared to numerical simulations of the ignition by an electrical discharge. To provide the correct initial conditions and arrive at meaningful results, the discharge characteristics will need to be explored in more detail in an experiment.

CRediT authorship contribution statement

Stefan Essmann: Conceptualization, Methodology, Project administration, Resources, Supervision, Writing – original draft, Writing – review & editing. **Jessica Dymke:** Investigation, Methodology, Visualization, Writing – review & editing, Conceptualization, Data curation, Formal analysis, Writing – original draft. **Jacqueline Höltkemeier-Horstmann:** Data curation, Investigation, Software, Visualization, Writing – review & editing. **Dieter Möckel:** Conceptualization, Resources, Supervision. **Carola Schierding:** Conceptualization, Resources, Writing – review & editing. **Michael Hilbert:** Conceptualization, Methodology, Supervision, Writing – review & editing. **Chunkan Yu:** Writing – review & editing. **Ulrich Maas:** Writing – review & editing. **Detlev Markus:** Conceptualization, Project administration, Supervision, Writing – review & editing.

Declaration of competing interest

The authors declare that they have no known competing financial interests or personal relationships that could have appeared to influence the work reported in this paper.

Data availability

Data will be made available on request.

Acknowledgements

This research did not receive any specific grant from funding agencies in the public, commercial, or not-for-profit sectors.

Appendix A. Supplementary data

Supplementary material related to this article can be found online at https://doi.org/10.1016/j.jaecs.2024.100254.

References

[1] Valera-Medina A, Amer-Hatem F, Azad AK, Dedoussi IC, de Joannon M, Fernandes RX, et al. Review on ammonia as a potential fuel: From synthesis to economics. Energy Fuels 2021. http://dx.doi.org/10.1021/acs.energyfuels.0c03685.

[2] Pfennig M, Böttger D, Häckner B, Geiger D, Zink C, Bisevic A, et al. Global GIS-based potential analysis and cost assessment of Power-to-X fuels in 2050. 2022, http://dx.doi.org/10.48550/arXiv.2208.14887.

[3] Valera-Medina A, Xiao H, Owen-Jones M, David W, Bowen PJ. Ammonia for power. Prog Energy Combust Sci 2018;69:63–102. http://dx.doi.org/10.1016/j.pecs.2018.07.001.

[4] MacFarlane DR, Cherepanov PV, Choi J, Suryanto BH, Hodgetts RY, Bakker JM, et al. A roadmap to the ammonia economy. Joule 2020;4(6):1186–205. http://dx.doi.org/10.1016/j.joule.2020.04.004.

[5] Lesmana H, Zhang Z, Li X, Zhu M, Xu W, Zhang D. NH_3 as a transport fuel in internal combustion engines: A technical review. J Energy Resour Technol 2019;141(7). http://dx.doi.org/10.1115/1.4042915.

[6] Kobayashi H, Hayakawa A, Somarathne KKA, Okafor EC. Science and technology of ammonia combustion. Proc Combust Inst 2019;37(1):109–33. http://dx.doi.org/10.1016/j.proci.2018.09.029.

[7] Berwal P, Kumar S, Khandelwal B. A comprehensive review on synthesis, chemical kinetics, and practical application of ammonia as future fuel for combustion. J Energy Inst 2021;99:273–98. http://dx.doi.org/10.1016/j.joei.2021.10.001.

[8] Elbaz AM, Wang S, Guiberti TF, Roberts WL. Review on the recent advances on ammonia combustion from the fundamentals to the applications. Fuel Commun 2022;10:100053. http://dx.doi.org/10.1016/j.jfueco.2022.100053.

[9] Herbinet O, Bartocci P, Grinberg Dana A. On the use of ammonia as a fuel – A perspective. Fuel Commun 2022;11:100064. http://dx.doi.org/10.1016/j.jfueco.2022.100064.

[10] Li J, Lai S, Chen D, Wu R, Kobayashi N, Deng L, et al. A review on combustion characteristics of ammonia as a carbon-free fuel. Front Energy Res 2021;9. http://dx.doi.org/10.3389/fenrg.2021.760356.

[11] Lhuillier C, Brequigny P, Lamoureux N, Contino F, Mounaïm-Rousselle C. Experimental investigation on laminar burning velocities of ammonia/hydrogen/air mixtures at elevated temperatures. Fuel 2020;263:116653. http://dx.doi.org/10.1016/j.fuel.2019.116653.

[12] Shrestha KP, Lhuillier C, Barbosa AA, Brequigny P, Contino F, Mounaïm-Rousselle C, et al. An experimental and modeling study of ammonia with enriched oxygen content and ammonia/hydrogen laminar flame speed at elevated pressure and temperature. Proc Combust Inst 2021;38(2):2163–74. http://dx.doi.org/10.1016/j.proci.2020.06.197.

[13] Zitouni S, Brequigny P, Mounaïm-Rousselle C. Influence of hydrogen and methane addition in laminar ammonia premixed flame on burning velocity, Lewis number and Markstein length. Combust Flame 2023;253:112786. http://dx.doi.org/10.1016/j.combustflame.2023.112786.

[14] Sileghem L, Alekseev VA, Vancoillie J, van Geem KM, Nilsson E, Verhelst S, Konnov AA. Laminar burning velocity of gasoline and the gasoline surrogate components iso-octane, n-heptane and toluene. Fuel 2013;112:355–65. http://dx.doi.org/10.1016/j.fuel.2013.05.049.

[15] Ichikawa A, Hayakawa A, Kitagawa Y, Kunkuma Amila Somarathne KD, Kudo T, Kobayashi H. Laminar burning velocity and Markstein length of ammonia/hydrogen/air premixed flames at elevated pressures. Int J Hydrog Energy 2015;40(30):9570–8. http://dx.doi.org/10.1016/j.ijhydene.2015.04.024.

[16] Mashruk S, Vigueras-Zuniga MO, Tejeda-del Cueto ME, Xiao H, Yu C, Maas U, et al. Combustion features of $CH_4/NH_3/H_2$ ternary blends. Int J Hydrog Energy 2022;47(70):30315–27. http://dx.doi.org/10.1016/j.ijhydene.2022.03.254.

[17] Warnatz J. Resolution of gas phase and surface combustion chemistry into elementary reactions. Symp (Int) Combust 1992;24(1):553–79. http://dx.doi.org/10.1016/S0082-0784(06)80070-6.

[18] Chen J, Jiang X, Qin X, Huang Z. Effect of hydrogen blending on the high temperature auto-ignition of ammonia at elevated pressure. Fuel 2021;287:119563. http://dx.doi.org/10.1016/j.fuel.2020.119563.

[19] Han X, Wang Z, Costa M, Sun Z, He Y, Cen K. Experimental and kinetic modeling study of laminar burning velocities of NH_3/air, NH_3/H_2/air, NH_3/CO/air and NH_3/CH_4/air premixed flames. Combust Flame 2019;206:214–26. http://dx.doi.org/10.1016/j.combustflame.2019.05.003.

[20] Yu C, Eckart S, Essmann S, Markus D, Valera-Medina A, Schießl R, et al. Investigation of spark ignition processes of laminar strained premixed stoichiometric NH_3-H_2-air flames. J Loss Prev Process Ind 2023;83:105043. http://dx.doi.org/10.1016/j.jlp.2023.105043.

[21] Lhuillier C, Brequigny P, Contino F, Mounaïm-Rousselle C. Experimental study on ammonia/hydrogen/air combustion in spark ignition engine conditions. Fuel 2020;269:117448.

[22] Fernández-Tarrazo E, Gómez-Miguel R, Sánchez-Sanz M. Minimum ignition energy of hydrogen–ammonia blends in air. Fuel 2023;337:127128. http://dx.doi.org/10.1016/j.fuel.2022.127128.

[23] Verkamp FJ, Hardin MC, Williams JR. Ammonia combustion properties and performance in gas-turbine burners. Symp (Int) Combust 1967;11(1):985–92. http://dx.doi.org/10.1016/S0082-0784(67)80225-X.

[24] Buckley WL, Husa HW. Combustion properties of ammonia. Chem Eng Prog 1962;58(2):81–4.

[25] Harris GFP, MacDermott PE. Flammability and explosibility of ammonia. In: iChemE symposium series 49. 1977, p. 29–36.

[26] Krämer H. Minimum ignition energy of ammonia/air atmosphere. In: GD 85. Leeds: Univ. Press; 1985, p. 504–6.

[27] Davis SG, Pagliaro JL, Debold TF, van Wingerden M, van Wingerden K. Flammability and explosion characteristics of mildly flammable refrigerants. J Loss Prev Process Ind 2017;49:662–74. http://dx.doi.org/10.1016/j.jlp.2017.05.019.

[28] Sadaghiani MS, Arami-Niya A, Zhang D, Tsuji T, Tanaka Y, Seiki Y, et al. Minimum ignition energies and laminar burning velocities of ammonia, HFO-1234yf, HFC-32 and their mixtures with carbon dioxide, HFC-125 and HFC-134a. J Hazard Mater 2021;407:124781. http://dx.doi.org/10.1016/j.jhazmat.2020.124781.

[29] Lesmana H, Zhu M, Zhang Z, Gao J, Wu J, Zhang D. An experimental investigation into the effect of spark gap and duration on minimum ignition energy of partially dissociated NH_3 in air. Combust Flame 2022;241:112053. http://dx.doi.org/10.1016/j.combustflame.2022.112053.

[30] Pfahl U, Ross M, Shepherd J, Pasamehmetoglu K, Unal C. Flammability limits, ignition energy, and flame speeds in H_2–CH_4–NH_3–N_2O–O_2–N_2 mixtures. Combust Flame 2000;123(1–2):140–58. http://dx.doi.org/10.1016/S0010-2180(00)00152-8.

[31] Oh S, Park C, Kim S, Kim Y, Choi Y, Kim C. Natural gas–ammonia dual-fuel combustion in spark-ignited engine with various air–fuel ratios and split ratios of ammonia under part load condition. Fuel 2021;290:120095. http://dx.doi.org/10.1016/j.fuel.2020.120095.

[32] Maly R. Spark ignition: its physics and effect on the internal combustion engine. In: Hilliard JC, Springer GS, editors. Fuel economy in road vehicles powered by spark ignition engines. New York: Plenum Press; 1984, p. 91–148. http://dx.doi.org/10.1007/978-1-4899-2277-9_3.

[33] Essmann S, Markus D, Maas U. Investigation of the spark channel of electrical discharges near the minimum ignition energy. Plasma Phys Technol 2016;3(3):116–21.

[34] Essmann S, Markus D, Grosshans H, Maas U. Experimental investigation of the stochastic early flame propagation after ignition by a low-energy electrical discharge. Combust Flame 2020;211:44–53. http://dx.doi.org/10.1016/j.combustflame.2019.09.021.

[35] Kono M, Kumagai S, Sakai T. The optimum condition for ignition of gases by composite sparks. Symp (Int) Combust 1977;16:757–66. http://dx.doi.org/10.1016/S0082-0784(77)80369-X.

[36] E27 Committee. ASTM E582-21: Test method for minimum ignition energy and quenching distance in gaseous mixtures. 2021, http://dx.doi.org/10.1520/E0582-21.

[37] PTB, BAM. Chemsafe: Database for safety characteristics in explosion protection. 2023, URL www.chemsafe.ptb.de.

[38] Li H, Xiao H, Sun J. Laminar burning velocity, Markstein length, and cellular instability of spherically propagating NH_3/H_2/Air premixed flames at moderate pressures. Combust Flame 2022;241:112079. http://dx.doi.org/10.1016/j.combustflame.2022.112079.

[39] Mørch CS, Bjerre A, Gøttrup MP, Sorenson SC, Schramm J. Ammonia/hydrogen mixtures in an SI-engine: Engine performance and analysis of a proposed fuel system. Fuel 2011;90(2):854–64. http://dx.doi.org/10.1016/j.fuel.2010.09.042.

[40] Duynslaegher C. Experimental and numerical study of ammonia combustion [Ph.D. thesis], Louvain: Université catholique; 2011.

[41] Pochet M, Truedsson I, Foucher F, Jeanmart H, Contino F. Ammonia-hydrogen blends in homogeneous-charge compression-ignition engine. In: SAE technical paper series. Warrendale, PA, United States: SAE International400 Commonwealth Drive; 2017, http://dx.doi.org/10.4271/2017-24-0087.

[42] Valera-Medina A, Pugh DG, Marsh P, Bulat G, Bowen P. Preliminary study on lean premixed combustion of ammonia-hydrogen for swirling gas turbine combustors. Int J Hydrog Energy 2017;42(38):24495–503. http://dx.doi.org/10.1016/j.ijhydene.2017.08.028.

[43] Goodwin DG, Moffat HK, Schoegl I, Speth RL, Weber BW. Cantera: An object-oriented software toolkit for chemical kinetics, thermodynamics, and transport processes. 2022, http://dx.doi.org/10.5281/zenodo.6387882, Version 2.6.0, https://www.cantera.org.

[44] Okafor EC, Hayakawa A, Nagano Y, Kitagawa T. Effects of hydrogen concentration on premixed laminar flames of hydrogen–methane–air. Int J Hydrog Energy 2014;39(5):2409–17. http://dx.doi.org/10.1016/j.ijhydene.2013.11.128.

[45] Göttgens J, Mauss F, Peters N. Analytic approximations of burning velocities and flame thicknesses of lean hydrogen, methane, ethylene, ethane, acetylene, and propane flames. Symp (Int) Combust 1992;24(1):129–35. http://dx.doi.org/10.1016/S0082-0784(06)80020-2.

[46] Matalon M, Cui C, Bechtold JK. Hydrodynamic theory of premixed flames: Effects of stoichiometry, variable transport coefficients and arbitrary reaction orders. J Fluid Mech 2003;487:179–210. http://dx.doi.org/10.1017/S0022112003004683.

[47] Chen Z, Burke MP, Ju Y. Effects of lewis number and ignition energy on the determination of laminar flame speed using propagating spherical flames. Proc Combust Inst 2009;32(1):1253–60. http://dx.doi.org/10.1016/j.proci.2008.05.060.

[48] Bechtold JK, Matalon M. The dependence of the markstein length on stoichiometry. Combust Flame 2001;127(1–2):1906–13. http://dx.doi.org/10.1016/S0010-2180(01)00297-8.

[49] Addabbo R, Bechtold JK, Matalon M. Wrinkling of spherically expanding flames. Proc Combust Inst 2002;29(2):1527–35. http://dx.doi.org/10.1016/S1540-7489(02)80187-0.

[50] Dinkelacker F, Manickam B, Muppala S. Modelling and simulation of lean premixed turbulent methane/hydrogen/air flames with an effective lewis number approach. Combust Flame 2011;158(9):1742–9. http://dx.doi.org/10.1016/j.combustflame.2010.12.003.

[51] Müller UC, Bollig M, Peters N. Approximations for burning velocities and markstein numbers for lean hydrocarbon and methanol flames. Combust Flame 1997;108(3):349–56. http://dx.doi.org/10.1016/S0010-2180(96)00110-1.

[52] Bouvet N, Halter F, Chauveau C, Yoon Y. On the effective lewis number formulations for lean hydrogen/hydrocarbon/air mixtures. Int J Hydrogen Energy 2013;38(14):5949–60. http://dx.doi.org/10.1016/j.ijhydene.2013.02.098.

[53] Wang Z, Ji C, Wang D, Hou R, Zhang T, Wang S. Experimental and numerical study on premixed partially dissociated ammonia mixtures. Part II: Numerical study of premixed combustion characteristics. Fuel 2021;306:121660. http://dx.doi.org/10.1016/j.fuel.2021.121660.

[54] Lewis B, von Elbe G. Combustion, flames and explosions of gases. 3rd ed. Orlando: Academic Press; 1987.

[55] Bane SP, Ziegler JL, Shepherd JE. Investigation of the effect of electrode geometry on spark ignition. Combust Flame 2015;162(2):462–9. http://dx.doi.org/10.1016/j.combustflame.2014.07.017.

[56] Wähner A, Gramse G, Langer T, Beyer M. Determination of the minimum ignition energy on the basis of a statistical approach. J Loss Prev Process Ind 2013;26(6):1655–60. http://dx.doi.org/10.1016/j.jlp.2013.06.002.

[57] Huber M, Harvey A, Lemmon E, Hardin G, Bell I, McLinden M. NIST reference fluid thermodynamic and transport properties database (REFPROP) Version 10 - SRD 23. 2018, http://dx.doi.org/10.18434/T4/1502528.

[58] Hattwig M, Steen H. handbook of explosion prevention and protection. Weinheim: Wiley-VCH; 2004.

[59] Krause T, Meier M, Brunzendorf J. Influence of thermal shock of piezoelectric pressure sensors on the measurement of explosion pressures. J Loss Prev Process Ind 2021;71:104523. http://dx.doi.org/10.1016/j.jlp.2021.104523.

[60] Krause T, Kanbur H, Springer N, Brunzendorf J, Markus D, Walch O, et al. Acceleration sensitivity of piezoelectric pressure sensors and the influence on the measurement of explosion pressures. J Loss Prev Process Ind 2023;82:104999. http://dx.doi.org/10.1016/j.jlp.2023.104999.

[61] Xu DA, Shneider MN, Lacoste DA, Laux CO. Thermal and hydrodynamic effects of nanosecond discharges in atmospheric pressure air. J Phys D: Appl Phys 2014;47(23). http://dx.doi.org/10.1088/0022-3727/47/23/235202.

[62] European Committee for Standardization. EN 15967:2022-03: Determination of maximum explosion pressure and the maximum rate of pressure rise of gases and vapours. 2022.
[63] Di Sarli V, Cammarota F, Salzano E, Di Benedetto A. Explosion behavior of ammonia and ammonia/methane in oxygen-enriched air. Process Saf Prog 2017;36(4):368–71. http://dx.doi.org/10.1002/prs.11912.
[64] Li Y, Bi M, Li B, Zhou Y, Huang L, Gao W. Explosion hazard evaluation of renewable hydrogen/ammonia/air fuels. Energy 2018;159:252–63. http://dx.doi.org/10.1016/j.energy.2018.06.174.
[65] Eisazadeh-Far K, Parsinejad F, Metghalchi H, Keck JC. On flame kernel formation and propagation in premixed gases. Combust Flame 2010;157(12):2211–21. http://dx.doi.org/10.1016/j.combustflame.2010.07.016.
[66] Singh B, Rajendran LK, Bane SP, Vlachos P. Characterization of fluid motion induced by nanosecond spark plasmas: Using particle image velocimetry and background oriented schlieren. In: 2018 AIAA aerospace sciences meeting. Reston, Virginia: American Institute of Aeronautics and Astronautics; 2018, p. 42. http://dx.doi.org/10.2514/6.2018-0680.
[67] Singh B, Rajendran LK, Zhang J, Vlachos PP, Bane SPM. Vortex rings drive entrainment and cooling in flow induced by a spark discharge. Phys Rev Fluids 2020;5(11). http://dx.doi.org/10.1103/PhysRevFluids.5.114501.
[68] Singh B, Rajendran LK, Giarra M, Vlachos PP, Bane SPM. Measurement of the flow field induced by a spark plasma using particle image velocimetry. Exp Fluids 2018;59(12). http://dx.doi.org/10.1007/s00348-018-2632-y.
[69] Bradley D, Lung FK-K. Spark ignition and the early stages of turbulent flame propagation. Combust Flame 1987;69(1):71–93. http://dx.doi.org/10.1016/0010-2180(87)90022-8.
[70] Beeckmann J, Hesse R, Schaback J, Pitsch H, Varea E, Chaumeix N. Flame propagation speed and markstein length of spherically expanding flames: Assessment of extrapolation and measurement techniques. Proc Combust Inst 2019;37(2):1521–8. http://dx.doi.org/10.1016/j.proci.2018.08.047.
[71] Zhou M, Li G, Liang J, Ding H, Zhang Z. Effect of ignition energy on the uncertainty in the determination of laminar flame speed using outwardly propagating spherical flames. Proc Combust Inst 2019;37(2):1615–22. http://dx.doi.org/10.1016/j.proci.2018.07.084.